

Magnetic properties of BaCdVO(PO₄)₂: a strongly frustrated spin-1/2 square lattice close to the quantum critical regime

R. Nath,^{1,*} A. A. Tsirlin,^{1,2,†} H. Rosner,¹ and C. Geibel¹

¹Max Planck Institute for Chemical Physics of Solids, Nöthnitzer Str. 40, 01187 Dresden, Germany

²Department of Chemistry, Moscow State University, 119992 Moscow, Russia

We report magnetization and specific heat measurements on polycrystalline samples of BaCdVO(PO₄)₂ and show that this compound is a $S = 1/2$ frustrated square lattice with ferromagnetic nearest-neighbor (J_1) and antiferromagnetic next-nearest-neighbor (J_2) interactions. The coupling constants $J_1 \simeq -3.6$ K and $J_2 \simeq 3.2$ K are determined from a fitting of the susceptibility data and confirmed by an analysis of the saturation field ($\mu_0 H_s = 4.2$ T), the specific heat, and the magnetic entropy. BaCdVO(PO₄)₂ undergoes magnetic ordering at about 1 K, likely towards a columnar antiferromagnetic state. We find that BaCdVO(PO₄)₂ with the frustration ratio $\alpha = J_2/J_1 \simeq -0.9$ is closer to a critical (quantum spin liquid) region of the frustrated square lattice than any of the previously reported compounds. Positive curvature of the magnetization curve is observed in agreement with recent theoretical predictions for high-field properties of the frustrated square lattice close to the critical regime.

PACS numbers: 75.50.-y, 75.40.Cx, 75.30.Et, 75.10.Jm

I. INTRODUCTION

Low-dimensional spin systems are one of the actively studied subjects in solid state physics due to the possibility to observe numerous quantum phenomena and to interpret these phenomena within relatively simple models (e.g., Ising or Heisenberg models for different lattice types). An interesting phenomenon in the spin physics is the formation of a spin liquid – a strongly correlated ground state lacking long-range magnetic order. This ground state is usually related to the electronic mechanism of superconductivity suggested for high- T_c cuprates.^{1,2} Spin liquids originate from quantum fluctuations that are particularly strong in systems with reduced dimensionality and low spin value. The fluctuations can be further enhanced by introducing magnetic frustration which impedes long-range ordering of the system.

The spin-1/2 frustrated square lattice (FSL) is one of the simplest models giving rise to a spin liquid ground state. In this model (also known as the $J_1 - J_2$ model), magnetic moments on a square-lattice are subjected to nearest-neighbor interaction J_1 along the side of the square and next-nearest-neighbor interaction J_2 along the diagonal of the square. The FSL model is described by the frustration ratio $\alpha = J_2/J_1$ or, alternatively, by the frustration angle $\varphi = \tan^{-1}(J_2/J_1)$. Defining the thermodynamic energy scale of exchange couplings as $J_c = \sqrt{J_1^2 + J_2^2}$, one obtains $J_1 = J_c \cos \varphi$ and $J_2 = J_c \sin \varphi$ (see Fig. 1 and Ref. 3).

Extensive theoretical research on the FSL model has been done in the past. Initially, the studies were focused on the AFM region ($J_1, J_2 > 0$),^{4,5,6,7} while the general case (arbitrary signs for J_1 and J_2) was only considered quite recently.^{3,8,9,10,11} The phase diagram of the model (Fig. 1) includes three regions with different ordered phases: ferromagnet [FM, wave vector $\mathbf{Q} = (0, 0)$], Néel antiferromagnet [NAF, $\mathbf{Q} = (\pi, \pi)$],

and columnar antiferromagnet¹² [CAF, $\mathbf{Q} = (\pi, 0)$ or $(0, \pi)$]. Classically, first-order phase transitions should occur at the NAF-CAF ($\alpha = 0.5$) and the CAF-FM ($\alpha = -0.5$) boundaries. However, quantum fluctuations destroy long-range ordering, leading to the formation of critical regions with disordered ground states. In general, the ground state in the critical regions is referred to a quantum spin liquid (QSL) regime, but the particular nature of the spin liquid phases is still under discussion. A gapless nematic state is suggested for $\alpha \sim -0.5$,⁸ while different dimer phases (including resonating-valence-bond-type ones) are claimed to exist

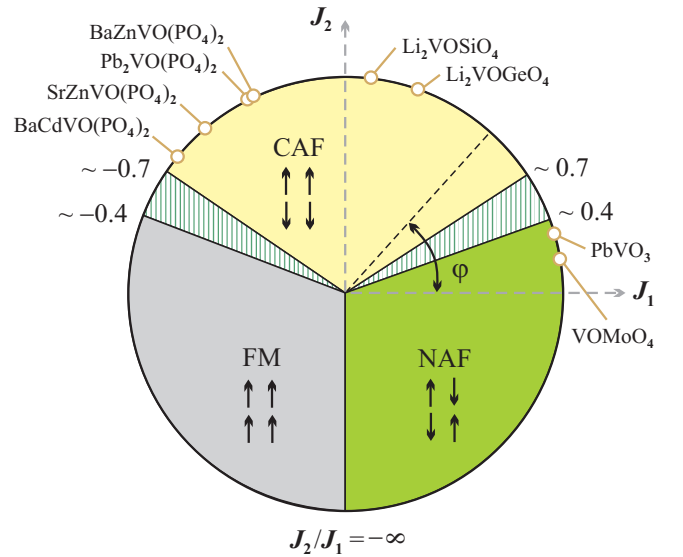


FIG. 1: (Color online) Phase diagram of the FSL model.⁹ Solid filling indicates the regions of long-range magnetic ordering, while hatched filling denotes the critical regions. Positions of BaCdVO(PO₄)₂ and some of the previously investigated compounds are shown (see text for references).

for α close to 0.5.⁵ Note also that the boundaries of the critical regions are not known exactly: for example, an α range from 0.34 to 0.60 is reported in Ref. 5 for the spin-liquid regime, while a wider region (0.24 – 0.83) is suggested in Ref. 6.

Despite numerous theoretical investigations, experimental realizations of the $J_1 - J_2$ model are scarce. Layered vanadium oxides Li_2VOXO_4 ($X = \text{Si}, \text{Ge}$) and VOMoO_4 were the first examples of the FSL systems. Initially, these materials were ascribed to $\alpha \simeq 1$ region of the phase diagram, and frustration-driven structural distortions were conjectured on the basis of nuclear magnetic resonance (NMR) data.^{13,14,15} However, later studies revealed the lack of the structural distortions and established a different scenario for all three systems. Thus, Li_2VOXO_4 compounds fall into the CAF region with $\alpha \gg 1$,^{16,17,18} while VOMoO_4 lies in the NAF region with $\alpha \simeq 0.2$.¹⁹

Complex vanadium phosphates $\text{AA}'\text{VO}(\text{PO}_4)_2$ present another realization of the FSL model with ferromagnetic J_1 and antiferromagnetic J_2 as will be discussed in detail below. We should also mention two very recent propositions for the FSL systems. $(\text{CuX})\text{LaNb}_2\text{O}_7$ ($X = \text{Cl}, \text{Br}$) perovskite-type compounds were claimed to realize the $J_1 - J_2$ model with ferromagnetic J_1 and antiferromagnetic J_2 .^{20,21} However, the estimates of J 's from different experimental techniques are contradictory, and the validity of the FSL model for these systems is still unclear.²² The layered perovskite PbVO_3 also reveals an interesting square lattice system with $\alpha \sim 0.3$, i.e., quite close to the antiferromagnetic (AFM) critical region.^{23,24} However, the complicated preparation procedure strongly hampers detailed investigation of this compound. Thus, little experimental information about the critical regions of the FSL model is available, and the search for new FSL systems is still challenging.

Complex vanadium phosphates $\text{AA}'\text{VO}(\text{PO}_4)_2$ have layered crystal structures (Fig. 2) with square lattice-like arrangement of V^{+4} ($S = 1/2$) cations. $[\text{VOPO}_4]$ layers are formed by VO_5 square pyramids linked via PO_4 tetrahedra. The tetrahedra allow for superexchange interactions both along the side and along the diagonal of the square, hence the FSL-like spin system is formed. Metal cations and additional, isolated PO_4 tetrahedra are located between the layers. The layers are flexible towards buckling, therefore metal-oxygen distances can be tuned, and different metal cations can be accommodated within the structure. Magnetic properties of the compounds with $\text{AA}' = \text{Pb}_2, \text{SrZn}$, and BaZn have been recently investigated by means of thermodynamic measurements^{25,26} and neutron scattering.^{27,28} We found that all the compounds fall to the CAF region of the FSL phase diagram. They reveal ferromagnetic J_1 and antiferromagnetic J_2 with α varying from -1.8 ($\text{AA}' = \text{Pb}_2, \text{BaZn}$) to -1.1 ($\text{AA}' = \text{SrZn}$).

An advantage of studying vanadium phosphates is the low energy scale for the exchange couplings (below 10 K) that allows for high-field experiments providing addi-

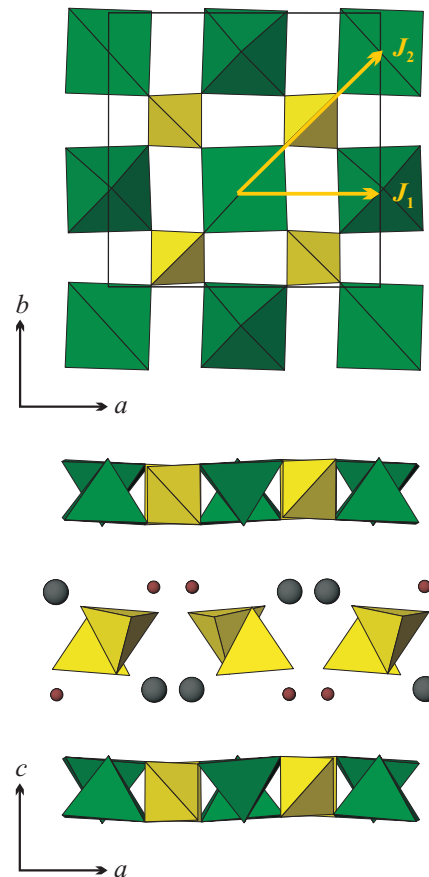


FIG. 2: (Color online) Crystal structure of $\text{BaCdVO}(\text{PO}_4)_2$: single $[\text{VOPO}_4]$ layer (upper panel) and stacking of the layers (bottom panel). Arrows indicate superexchange interactions J_1 (along the side of the square) and J_2 (along the diagonal of the square). Larger and smaller spheres denote Ba and Cd cations, respectively.

tional information about the properties of the system.¹¹ Yet there is also one complication. The crystal structures of $\text{AA}'\text{VO}(\text{PO}_4)_2$ do not have tetragonal symmetry; therefore, vanadium atoms do not form a regular square lattice. At first glance, the distortion of the square lattice is negligible. However, even a very slight alteration of the structure can lead to drastic changes in the exchange couplings as shown recently for $\text{Ag}_2\text{VOP}_2\text{O}_7$ (Ref. 29). In case of the $\text{AA}'\text{VO}(\text{PO}_4)_2$ compounds, we studied this issue in detail using band structure calculations and found considerable deviations from the square lattice model for some of the systems.³⁰ Nevertheless, the deviation is really negligible for one of the compounds – $\text{BaCdVO}(\text{PO}_4)_2$. Below, we present magnetic properties of this compound and interpret the results within the FSL model. A detailed examination of the appropriate spin models for other $\text{AA}'\text{VO}(\text{PO}_4)_2$ compounds will be published elsewhere.³⁰

The crystal structure of $\text{BaCdVO}(\text{PO}_4)_2$ has been reported by Meyer *et al.*,³¹ but magnetic properties of this compound were not investigated. In our work, we use a

set of different thermodynamic measurements to study magnetic interactions in $\text{BaCdVO}(\text{PO}_4)_2$. We show that $\text{BaCdVO}(\text{PO}_4)_2$ is a FSL system with the frustration ratio $\alpha \approx -0.9$, i.e., lying very close the critical region of the FSL.

The paper is organized as follows: Sec. II deals with the experimental details. In Sec. III, we present our results on $\text{BaCd}(\text{VO})(\text{PO}_4)_2$. Section IV contains a detailed discussion of the results in the light of the $J_1 - J_2$ model followed by our conclusions.

II. EXPERIMENTAL DETAILS

Polycrystalline samples of $\text{BaCd}(\text{VO})(\text{PO}_4)_2$ were prepared by solid state reaction technique using BaCO_3 , CdO , V_2O_3 , V_2O_5 , and $(\text{NH}_4)_2\text{HPO}_4$ as starting materials (all the chemicals had at least 99.9% purity grade). The process involved two steps. First, the intermediate compound BaCdP_2O_7 was prepared by firing the stoichiometric mixture of BaCO_3 and $(\text{NH}_4)_2\text{HPO}_4$ at 950°C in air for 48 h with one intermediate grinding. In the second step, stoichiometric amounts of BaCdP_2O_7 , V_2O_3 , and V_2O_5 were grinded, pelletized and annealed in dynamic vacuum (10^{-5} mbar) or evacuated and sealed quartz tube (10^{-2} mbar) at 800°C for 30 h.

The phase composition of the prepared samples was checked by x-ray diffraction (XRD) (Huber G670f camera, $\text{CuK}_{\alpha 1}$ radiation, ImagePlate detector). The samples contained $\text{BaCd}(\text{VO})(\text{PO}_4)_2$ and minor amount ($\sim 3\%$) of unreacted BaCdP_2O_7 . One then expects an equal amount of unreacted VO_2 to be present in the samples. However, a minor impurity of VO_2 can not be resolved by XRD due to the overlap of the strongest reflection of VO_2 with that of $\text{BaCdVO}(\text{PO}_4)_2$. Instead, a minor amount of the VO_2 impurity is evidenced by a small kink in the magnetic susceptibility data at 340 K (see Sec. III).

We tried to improve the quality of the samples by varying temperature and duration of the annealing. Unfortunately, $\text{BaCdVO}(\text{PO}_4)_2$ is rather unstable, and the formation of an unknown impurity phase was observed after long annealings at 800°C or any annealings above 800°C . The annealing at 900°C resulted in melting and complete decomposition (as seen by powder XRD) of the compound towards unknown phases.³² Regarding these difficulties, we did not attempt to grow single crystals of $\text{BaCdVO}(\text{PO}_4)_2$, because the data measured on polycrystalline samples are sufficient to determine the parameters of the FSL model and the location of the system within the phase diagram.

Magnetization (M) data were measured as a function of temperature using a SQUID magnetometer (Quantum Design MPMS). Specific heat $C_p(T)$ was measured on a pressed pellet with a standard relaxation technique using a Quantum Design PPMS. All the measurements were carried out over a wide temperature range ($0.4\text{ K} \leq T \leq 400\text{ K}$) and a field up to 7 T. The low-

temperature measurements were done partly using an additional ^3He setup.

III. RESULTS

Figure 3 shows the magnetic susceptibility $\chi = M/H$ of $\text{BaCdVO}(\text{PO}_4)_2$ as a function of temperature. At high temperature (above 20 K), the data behave in a Curie-Weiss (CW) manner. At lower temperature and low fields, the curve exhibits a broad maximum at $T_{\text{max}}^{\chi} \simeq 2.7\text{ K}$. The maximum is characteristic for low-dimensional spin systems and indicates a crossover to a state with antiferromagnetic correlations. A slight change of slope observed at $\sim 1\text{ K}$ is associated with magnetic ordering, while the Curie-like upturn in low fields below 1 K is likely caused by extrinsic paramagnetic impurities. An increase of the magnetic field leads to a shift of the maximum to lower temperatures, an increase of the χ value at the maximum (χ_{max}), and an increase of χ at the lowest investigated temperatures. This behavior is quite similar to that observed in the other FSL systems²⁶ and rather typical for low-dimensional and/or frustrated antiferromagnetic systems.

Careful examination reveals a small kink in $1/\chi$ vs. T curve at 340 K. This kink is indicative of the VO_2 impurity, since VO_2 undergoes metal-insulator transition at 340 K.³³ We emphasize that this impurity does not affect any of the results reported below, as the paramagnetic contribution of VO_2 below 300 K is temperature-independent, while the energy scale of the exchange interactions in $\text{BaCdVO}(\text{PO}_4)_2$ is lower by two orders of magnitude. However, the impurity prevents us from using the data above 300 K in further analysis.

High-temperature (20 – 300 K) susceptibility data can be fitted with a CW law corrected for the temperature-independent contribution χ_0 that accounts for diamagnetism of core shells and Van Vleck paramagnetism:

$$\chi(T) = \chi_0 + \frac{C}{T + \theta_{\text{CW}}} \quad (1)$$

The fitting resulted in $\chi_0 = -4.4(1) \times 10^{-4}$ emu/mol, $C = 0.375(2)$ emu K/mol, $\theta_{\text{CW}} = 0.66(4)$ K. This C value corresponds to an effective magnetic moment $\mu_{\text{eff}} = 1.73(1) \mu_B$ in perfect agreement with the expected spin-only value for V^{+4} . Note that θ_{CW} is slightly dependent on the lower limit of the data used due to the curvature in $1/\chi$ related to the maximum in $\chi(T)$. However, values of θ_{CW} below 1 K are obtained for any fit with a lower limit above 20 K.

Thus, we find a very low θ_{CW} value, despite the susceptibility maximum at $T_{\text{max}}^{\chi} \simeq 2.7\text{ K}$ indicates somewhat stronger exchange interactions. This result implies that several interactions with different signs are present in the system under investigation. To get a quantitative estimate of the exchange interactions, we fit the susceptibility data above 5 K with the high-temperature series

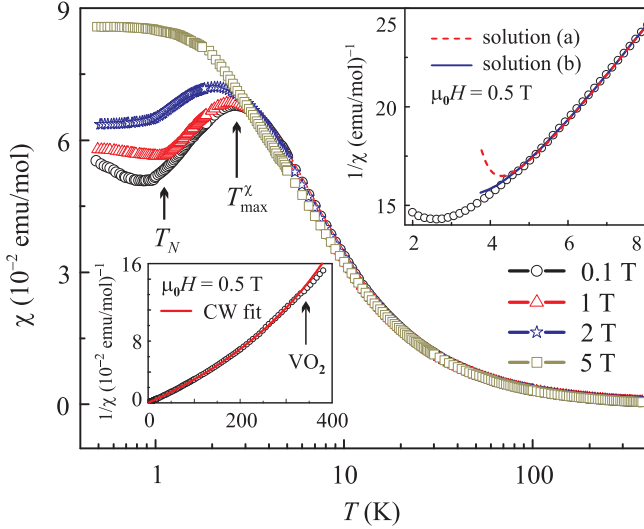


FIG. 3: (Color online) Temperature dependence of the susceptibility $\chi(T)$ of $\text{BaCd}(\text{VO})(\text{PO}_4)_2$ measured at different applied fields. Insets show inverse susceptibility (open circles) along with the HTSE [Eq. (2), upper inset] and the Curie-Weiss [Eq. (1), lower inset] fits. In the upper inset, dashed and solid lines denote solutions (a) and (b), respectively. In the lower inset, solid line is the Curie-Weiss fit, while the arrow indicates the kink at 340 K due to the VO_2 impurity.

expansion (HTSE) for the FSL model:¹⁷

$$\chi(T) = \chi_0 + \frac{N_A g^2 \mu_B^2}{k_B T} \sum_n \left(\frac{J_1}{k_B T} \right)^n \sum_m c_{m,n} \left(\frac{J_2}{J_1} \right)^m, \quad (2)$$

where χ_0 is temperature-independent contribution, g is Lande g -factor, and $c_{m,n}$ are the coefficients listed in Table I of Ref. 17. We find $\chi_0 = -3.8(2) \times 10^{-4}$ emu/mol, $g = 1.968(3)$, $J_1 = -3.62(5)$ K, and $J_2 = 3.18(2)$ K [solution (a)], or, alternatively, $\chi_0 = -3.9(2) \times 10^{-4}$ emu/mol, $g = 1.981(3)$, $J_1 = 2.16(1)$ K, and $J_2 = -2.05(4)$ K [solution (b)].³⁴ The fit with the solution (b) looks somewhat better and extends to lower temperatures as compared to the fit with the solution (a) (see the upper inset of Fig. 3). Therefore, one may speculate that the solution (b) is the correct one. However, the difference between the two fits is caused by the lower exchange couplings in the solution (b), since the HTSE is valid at $T \geq J_i$. In the region used for the fitting (above 5 K), both the solutions produce the fits of similar quality, hence they are indistinguishable. The solution (a) locates the system in the CAF region close to the FM critical region (i.e., the region on the CAF-FM boundary), while the solution (b) corresponds to a position deep into the stable NAF region. The presence of two solutions in fitting $\chi(T)$ with the HTSE for the FSL is a well-known problem. The ambiguity has to be resolved by the use of other experimental data.

To discriminate the valid set of J 's, we turn to magnetization data and analyze the value of the saturation

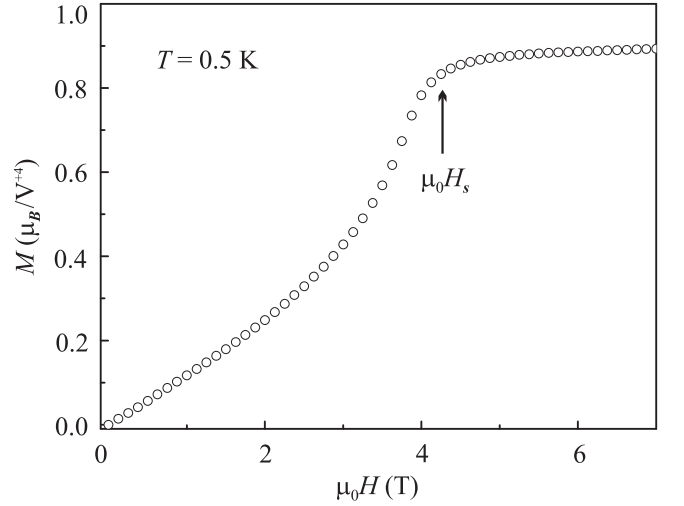


FIG. 4: Magnetization (M) as a function of the applied field (H) measured at 0.5 K – well below T_N . The arrow marks the saturation field $\mu_0 H_s$.

field H_s . According to theoretical results by Schmidt *et al.*,⁹ the saturation field can be calculated as

$$\mu_0 H_s = \frac{J_c k_B z S}{g \mu_B} \left[\left(1 - \frac{1}{2} (\cos Q_x + \cos Q_y) \right) \cos \varphi + (1 - \cos Q_x \cos Q_y) \sin \varphi \right], \quad (3)$$

where $z = 4$ (magnetic coordination number), $S = 1/2$ is the spin value, φ and J_c are defined in Section I, and (Q_x, Q_y) is the wave vector of the ordered state. Using the appropriate wave vectors for the CAF and NAF regions, one finds $\mu_0 H_s = 2(J_1 + 2J_2)k_B/(g\mu_B)$ for CAF and $4J_1 k_B/(g\mu_B)$ for NAF phases. The first set of J 's [solution (a)] results in $\mu_0 H_s = 4.2$ T, while the second set [solution (b)] gives rise to a much higher saturation field $\mu_0 H_s = 6.55$ T.

Figure 4 presents the magnetization curve measured at 0.5 K, i.e., well below the ordering temperature T_N . At low fields, the $M(H)$ dependence is linear, while a positive curvature is observed above 2 T leading to a marked kink at the saturation field $\mu_0 H_s \simeq 4.2$ T.³⁵ The saturation magnetization $M_s \simeq 0.9 \mu_B/V^{+4}$ is slightly less than the expected value of $1 \mu_B$. The reduction of M_s is likely caused by the weight error due to the presence of non-magnetic impurity (BaCdP_2O_7) in the samples under investigation (see Sec. II).³⁶ The curvature above 2 T is also somewhat puzzling. At first glance, one may interpret it as a spin-flop transition. However, the magnetic anisotropy of V^{+4} is weak. Thus, a spin-flop transition in $\text{Pb}_2\text{VO}(\text{PO}_4)_2$ is observed at 1 T,²⁶ and a strong increase of the anisotropy in the isostructural $\text{BaCdVO}(\text{PO}_4)_2$ compound is unlikely. In the next section, we will suggest an alternative and plausible explanation for the curvature of the $M(H)$ dependence above 2 T.

The experimentally determined saturation field matches exactly the value calculated for the solution

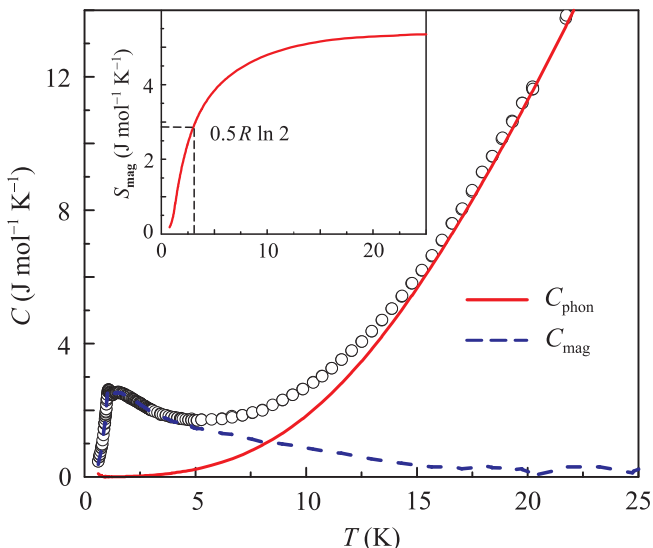


FIG. 5: (Color online) Temperature dependence of the specific heat $C_p(T)$ of $\text{BaCd}(\text{VO})(\text{PO}_4)_2$ measured at zero applied field. Open circles are the raw data, the solid line shows the phonon contribution [according to the fit with Eq. (4)], and the dashed line indicates the magnetic contribution C_{mag} . The anomaly at $T_N \simeq 1$ K is shown in detail in Fig. 6. In the inset, the magnetic entropy (S_{mag}) is plotted as a function of temperature, dashed lines show the entropy of $0.5R \ln 2$ and the respective temperature.

(a) of the susceptibility fit but is far below the value expected for the solution (b). This clearly demonstrates that the solution (a), with a ferromagnetic J_1 and an antiferromagnetic J_2 is the correct one. Thus, $\text{BaCdVO}(\text{PO}_4)_2$ belongs to the frustrated ferromagnetic square lattice system as all the other $\text{AA}'\text{VO}(\text{PO}_4)_2$ structural homologs.

Specific heat (C_p) measurement at zero field is shown in Fig. 5. At high temperatures, C_p is completely dominated by phonon excitations. Below 5 K, a decrease of temperature is accompanied by an increase of C_p indicating that the magnetic contribution to the specific heat becomes prominent. At low temperatures, $C_p(T)$ shows a broad maximum at $T_{\text{max}}^C \simeq 1.5$ K due to the spin correlations and a small but well resolved peak at $T_N \simeq 1$ K associated with the magnetic ordering (see also Fig. 6). Below T_N , $C_p(T)$ drops rapidly.

To extract the magnetic contribution to the specific heat C_{mag} , we subtract an estimated phonon contribution from the total measured specific heat C_p . For this purpose, the experimental data at high temperatures ($15 \text{ K} \leq T \leq 200 \text{ K}$) were fitted with

$$C_p(T) = \frac{A}{T^2} + 9R \sum_{n=1}^{n=4} c_n \left(\frac{T}{\theta_D^{(n)}} \right)^3 \int_0^{\theta_D^{(n)}/T} \frac{x^4 e^x}{(e^x - 1)^2} dx, \quad (4)$$

where A/T^2 accounts for the magnetic contribution at high temperatures, $R = 8.314 \text{ J/mol K}$ is the gas con-

stant, and the sum of Debye functions accounts for the phonon contribution. The use of several Debye functions with distinct characteristic temperatures $\theta_D^{(n)}$ is necessary due to the large difference in atomic masses of the elements forming the $\text{BaCdVO}(\text{PO}_4)_2$ compound. In general, the procedure is similar to that reported in Refs. 26, 37, and 38 for the related vanadium phosphates. The resulting $C_{\text{mag}}(T)$ curve is shown in Fig. 5. In the inset, we plot the temperature dependence of the magnetic entropy $S_{\text{mag}}(T)$ as obtained by integrating $C_{\text{mag}}(T)/T$. At high temperatures, $S_{\text{mag}}(T)$ converges towards the value $S_\infty \simeq 5.3 \text{ J/mol K}$, in reasonable agreement with the expected value $R \ln 2 = 5.76 \text{ J/mol K}$ taking into account the uncertainty in the estimated phonon contribution. The result indicates that C_{mag} reflects the intrinsic contribution of $\text{BaCdVO}(\text{PO}_4)_2$.

At the lowest limit ($T = 15 \text{ K}$) of the specific heat fit to Eq. (4), the magnetic contribution A/T^2 amounts to a small part of the total specific heat only. Therefore, the parameter A is obtained with a large uncertainty, $A = 100 \pm 30 \text{ J K/mol}$. The A/T^2 term corresponds to the lowest order in the HTSE for the specific heat¹⁷ and may be expressed as $A = 0.375J_c = 0.375R(J_1^2 + J_2^2)$. We find $A = 72 \text{ J K/mol}$ and $A = 29 \text{ J K/mol}$ using the J_i values of the solutions (a) and (b) of the susceptibility fit, respectively. Both theoretical values are below the experimental one, but the result for the solution (a) is still within the error bar, while that for the solution (b) is far below. Thus, this analysis also favors the solution (a) and the CAF scenario for $\text{BaCdVO}(\text{PO}_4)_2$.

A further rough estimate of the thermodynamic energy scale J_c can be obtained from the T -dependence of the magnetic entropy. In a general approximation, J_c is approximately twice the temperature at which the entropy reaches half of its high-temperature limit. In $\text{BaCdVO}(\text{PO}_4)_2$, $S(T) = 0.5R \ln 2$ at $T = 2.5 \text{ K}$. This temperature corresponds to $J_c = 5 \text{ K}$, in perfect agreement with the solution (a) ($J_c = 4.8 \text{ K}$), but in poor compliance with the solution (b) ($J_c = 3.0 \text{ K}$).

Field dependent specific heat measurements are presented in Fig. 6. The increase of the field results in the suppression of the broad maximum at 1.5 K, while the absolute value of C_p at T_N is enhanced. The maximum enhancement of the peak value is observed at 2 T where the transition anomaly is most pronounced. With further increase of the field, the peak value decreases again and the anomaly broadens slightly. However, between 3.5 and 4 T the anomaly gets completely suppressed. The variation of the transition temperature is as follows: T_N increases very slightly from 0 to 2 T up to a maximum $T_N(2 \text{ T}) = 1.1 \text{ K}$ and decreases more clearly with further increase of the field. This result enables to draw the $H-T$ phase diagram of the system (inset of Fig. 6). The field dependence of the specific heat is similar to that of $\text{Pb}_2\text{VO}(\text{PO}_4)_2$,²⁶ but the smaller energy scale of the exchange couplings facilitates experimental access to the larger part of the H vs. T phase diagram.

The field dependence may be understood as follows.

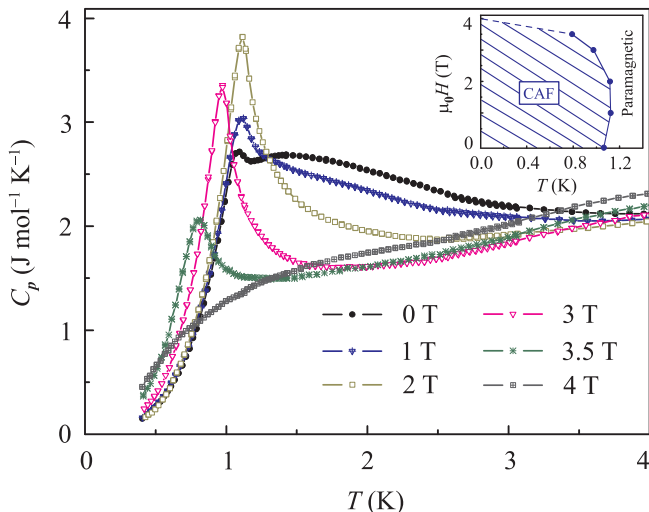


FIG. 6: Specific heat of $\text{BaCdVO}(\text{PO}_4)_2$ measured in different magnetic fields. The inset shows the $H-T$ phase diagram of the system.

The broad maximum at 1.5 K is caused by short-range antiferromagnetic correlations. These correlations are suppressed by the applied magnetic field, hence the maximum is strongly reduced already at 1 T. The magnetic entropy is transferred to the transition anomaly resulting in a much larger and sharper peak at T_N . As we have mentioned in the introduction, long-range magnetic ordering in low-dimensional and/or frustrated spin systems is suppressed by quantum fluctuations. Magnetic field suppresses these fluctuations, therefore T_N is slightly enhanced at low fields. However, above 2 T the field is strong enough to overcome the antiferromagnetic ordering, hence T_N is reduced and finally suppressed below 0.4 K at 4 T.

IV. DISCUSSION

Our experimental results and our analysis demonstrate that $\text{BaCdVO}(\text{PO}_4)_2$ is a frustrated square lattice with a ferromagnetic exchange J_1 along the side of the square and an antiferromagnetic exchange J_2 along the diagonal. The first evidence for the presence of antiferromagnetic and ferromagnetic exchange of similar size is given by the very small value of the Weiss constant $\theta_{\text{CW}} < 1$ K contrasting a much higher value of the temperature $T_{\text{max}}^{\chi} \simeq 2.7$ K of the maximum in $\chi(T)$. The latter one reflects the onset of antiferromagnetic correlations. In a non-frustrated $S = 1/2$ antiferromagnetic square lattice, this maximum is expected at $T_{\text{max}}^{\chi} = 0.95J$ (Refs. 39 and 40), suggesting some antiferromagnetic exchange with $J \gtrsim 3$ K in $\text{BaCdVO}(\text{PO}_4)_2$. Then a much smaller θ_{CW} , which is the sum of all the exchange interactions in the system under investigation, implies an additional exchange of the opposite sign and thus ferromagnetic.

A fit of the susceptibility in the T range 5 K \leq

$T \leq 300$ K with the HTSE for the FSL resulted in two sets of exchange coupling parameters: solution (a) with $J_1 \simeq -3.6$ K, $J_2 \simeq 3.2$ K and solution (b) with $J_1 \simeq 2.2$ K, $J_2 \simeq -2.1$ K. The two solutions correspond to different regions of the FSL phase diagram and realize the frustrated CAF and non-frustrated NAF regimes, respectively. Further experimental results enable to select (a) as the correct solution.

The frustrated regime of the solution (a) causes the low saturation field of $\mu_0 H_s = 4.2$ T. The non-frustrated ground state for the solution (b) corresponds to the higher saturation field of $\mu_0 H_s = 6.55$ T despite both J_1 and J_2 are weaker than in the solution (a). Magnetization measurements at low temperatures show a well defined saturation at the saturation field $\mu_0 H_s = 4.2$ T. This value matches perfectly the $\mu_0 H_s$ expected for the solution (a) but is well below the $\mu_0 H_s$ expected for the solution (b). Further on, an analysis of the magnetic specific heat at high temperatures (> 15 K) as well as of the T dependence of the magnetic entropy at low temperatures (< 3 K) leads to a thermodynamic energy scale of the exchange couplings J_c in reasonable agreement with the solution (a) but in clear disagreement with the solution (b). Therefore, the solution (a) is the appropriate one to describe the spin system of $\text{BaCdVO}(\text{PO}_4)_2$.

The solution (a) with $J_1 \simeq -3.6$ K and $J_2 \simeq 3.2$ K places the system to the CAF region of the FSL phase diagram. With $J_2/J_1 = -0.9$ corresponding to $\varphi/\pi = 0.76$, $\text{BaCdVO}(\text{PO}_4)_2$ is quite close to the border of the FM critical regime ($J_2/J_1 = -0.7$), closer than any of the previously reported FSL compounds such as $\text{SrZnVO}(\text{PO}_4)_2$ ($J_2/J_1 = -1.1$) and $\text{Pb}_2\text{VO}(\text{PO}_4)_2$ or $\text{BaZnVO}(\text{PO}_4)_2$ ($J_2/J_1 = -1.8$). A direct evidence for the strong frustration in $\text{BaCdVO}(\text{PO}_4)_2$ is given by the position of the specific heat maximum (T_{max}^C) and the maximum value of the magnetic specific heat (C_{max}). The specific heat of the FSL at low temperatures ($T < J_c$) is not known precisely, since there is presently no established way to compute it. However, for an unfrustrated square lattice, the value at the maximum seems nowadays to be established within a few percent, $C_{\text{max}} \simeq 0.46R = 3.82$ J/mol K at $T_{\text{max}}^C/J_1 = 0.60$.^{39,41} It is further established that tuning the FSL towards a critical region leads to a broadening of this maximum, a reduction of the C_{mag} value at the maximum, and a shift of the maximum towards lower temperatures. Such a trend was already observed in the previously studied FSL systems, where C_{max}/R and T_{max}^C/J_c are decreased from 0.46 and 0.6 in $\text{Li}_2\text{VOSiO}_4$ (far away from any critical region) towards 0.44 and 0.40 in $\text{Pb}_2\text{VO}(\text{PO}_4)_2$ and finally to 0.40 and 0.29 in $\text{SrZnVO}(\text{PO}_4)_2$ (closer to the critical region).²⁶

In $\text{BaCdVO}(\text{PO}_4)_2$, C_{max}/R reaches only 0.33, well below the value found in the other FSL systems, while $T_{\text{max}}^C/J_c = 0.31$. The very small value of C_{max} cannot be attributed to a scaling problem due to a large amount of a foreign phase, since the magnetic entropy at high temperatures is close to $R \ln 2$ (the phonon contribution at T_{max}^C amounts to less than 1% of the total specific heat and can

therefore safely be neglected). Further on, a comparison of $C_{\text{mag}}(T)$ near its maximum for different FSL systems using a reduced T/J_c temperature scale indicates that the maximum in $C_{\text{mag}}(T)$ of $\text{BaCdVO}(\text{PO}_4)_2$ is broader, and the decrease of $C_{\text{mag}}(T)$ above T_{max}^C is much weaker than in the other known FSL systems. Thus, this broad maximum with a small C_{mag} value at the maximum is also a direct experimental evidence for the strong frustration.

A further (and new) manifestation of the frustration is likely observed in our magnetization curve (Fig. 4). Above 2 T, the slope of $M(H)$ increases with magnetic field and steps up just before saturation is reached. Such a behavior has been recently predicted by theoretical calculations for the FSL.¹¹ This steeping up just below H_s is suggested to be more pronounced for systems that are close to the critical regions. However, further magnetization measurements on other FSL systems are needed to confirm this trend.

Using exact diagonalization of finite-size clusters, Shannon *et al.*³ calculated the dependence of a number of characteristic properties of the FSL (such as T_{max}^X , T_{max}^C , χ_{max} , and C_{max}) as a function of φ . Comparison of these predictions with the experimental observation for $\text{BaCdVO}(\text{PO}_4)_2$ and the related compounds indicates that while the overall φ dependence seems to be reproduced, the calculated absolute values are slightly too large. This difference is likely a consequence of the finite cluster size that leads to a gapped energy excitation spectra and thus an exponential vanishing of $C_{\text{mag}}(T)$ and $\chi(T)$ at very low T in contrast to the real behavior. The missing entropy has then to be recovered at higher temperatures, thus enhancing $C_{\text{mag}}(T)$ at its maximum and shifting the maximum to higher T .

A last comment on the antiferromagnetic order observed at $T_N \simeq 1.0$ K. The anomalies in $\chi(T)$ and $C_p(T)$

are much smaller than those expected for a classical three-dimensional magnetic system but very similar to those observed in the other FSL systems, e.g., $\text{Li}_2\text{VOSiO}_4$ (Refs. 14 and 26) or $\text{Pb}_2\text{VO}(\text{PO}_4)_2$ (Refs. 25 and 26). Since in some of these systems long-range magnetic order was directly confirmed by NMR or neutron scattering experiments,^{18,27,28} the similarity in the behavior allows us to safely claim that these small anomalies in $\chi(T)$ and $C_p(T)$ correspond to the onset of (columnar) antiferromagnetic order in $\text{BaCdVO}(\text{PO}_4)_2$ too. The ratio $R = T_N/T_{\text{max}}^X$ is smaller in $\text{BaCdVO}(\text{PO}_4)_2$ ($R = 0.39$) than in the other FSL systems ($0.4 < R < 0.6$), reflecting either the weakness of interlayer exchange and/or the suppression of the AFM order by quantum fluctuations.

In conclusion, our study of $\text{BaCdVO}(\text{PO}_4)_2$ shows that the magnetic properties of this compound are well understood within the FSL model. Magnetic susceptibility, magnetization, and specific heat data consistently suggest $J_1 \simeq -3.6$ K, $J_2 \simeq 3.2$ K, hence $\alpha \simeq -0.9$, locating the compound into the CAF region of the FSL phase diagram. $\text{BaCdVO}(\text{PO}_4)_2$ lies closer to the critical region of the FSL than any of the previously reported compounds. This conclusion is supported by a strongly reduced maximum of the magnetic specific heat and a positive curvature of the magnetization curve consistent with the recent theoretical predictions.

Acknowledgments

The authors are grateful to Nic Shannon and B. Schmidt for fruitful discussions. Financial support of GIF (Grant No. I-811-257.14/03), RFBR (Grant No. 07-03-00890), and the Emmy Noether program of the DFG is acknowledged.

* Electronic address: ramesh.phy2003@yahoo.com

† Electronic address: altsirlin@gmail.com

¹ P. W. Anderson, *Science* **235**, 1196 (1987).

² P. A. Lee, *Rep. Prog. Phys.* **71**, 012501 (2008).

³ N. Shannon, B. Schmidt, K. Penc, and P. Thalmeier, *Eur. Phys. J. B* **38**, 599 (2004); *cond-mat/0312160*.

⁴ P. Chandra and B. Doucot, *Phys. Rev. B* **38**, 9335 (1988).

⁵ O. P. Sushkov, J. Oitmaa, and Z. Weihong, *Phys. Rev. B* **63**, 104420 (2001); *cond-mat/0007329*, and references therein.

⁶ L. Siurakshina, D. Ihle, R. Hayn, *Phys. Rev. B* **64**, 104406 (2001), and references therein.

⁷ S. Bacci, E. Gagliano, and E. Dagotto, *Phys. Rev. B* **44**, 285 (1991).

⁸ N. Shannon, T. Momoi, and P. Sindzingre, *Phys. Rev. Lett.* **96**, 027213 (2006); *cond-mat/0512349*.

⁹ B. Schmidt, P. Thalmeier, and N. Shannon, *Phys. Rev. B* **76**, 125113 (2007); *arXiv:0705.3094*.

¹⁰ B. Schmidt, N. Shannon, and P. Thalmeier, *J. Phys.: Condens. Matter* **19**, 145211 (2007).

¹¹ P. Thalmeier, M. E. Zhitomirsky, B. Schmidt, and N. Shannon, *Phys. Rev. B* **77**, 104441 (2008); *arXiv:0711.4054*.

¹² Note that this phase is commonly named "collinear antiferromagnet", although the term is somewhat misleading.

¹³ R. Melzi, P. Carretta, A. Lascialfari, M. Mambrini, M. Troyer, P. Millet, and F. Mila, *Phys. Rev. Lett.* **85**, 1318 (2000); *cond-mat/0005273*.

¹⁴ R. Melzi, S. Aldrovandi, F. Tedoldi, P. Carretta, P. Millet, and F. Mila, *Phys. Rev. B* **64**, 024409 (2001); *cond-mat/0101066*.

¹⁵ P. Carretta, N. Papinutto, C. B. Azzoni, M. C. Mozzati, E. Pavarini, S. Gonthier, and P. Millet, *Phys. Rev. B* **66**, 094420 (2002).

¹⁶ H. Rosner, R. R. P. Singh, W. H. Zheng, J. Oitmaa, S.-L. Drechsler, and W. E. Pickett, *Phys. Rev. Lett.* **88**, 186405 (2002); *cond-mat/0110003*.

¹⁷ H. Rosner, R. R. P. Singh, W. H. Zheng, J. Oitmaa, and W. E. Pickett, *Phys. Rev. B* **67**, 014416 (2003).

¹⁸ A. Bombardi, J. Rodriguez-Carvajal, S. Di Matteo, F. de Bergevin, L. Paolasini, P. Carretta, P. Millet, and R. Caci-

- uffo, Phys. Rev. Lett. **93**, 027202 (2004).
- ¹⁹ A. Bombardi, L. C. Chapon, I. Margiolaki, C. Mazzoli, S. Gonthier, F. Duc, and P. G. Radaelli, Phys. Rev. B **71**, 220406(R) (2005).
- ²⁰ H. Kageyama, T. Kitano, N. Oba, M. Nishi, S. Nagai, K. Hirota, L. Viciu, J. B. Wiley, J. Yasuda, Y. Baba, Y. Ajiro, and K. Yoshimura, J. Phys. Soc. Jpn. **74**, 1702 (2005).
- ²¹ N. Oba, H. Kageyama, T. Kitano, J. Yasuda, Y. Baba, M. Nishi, K. Hirota, Y. Narumi, M. Hagiwara, K. Kindo, T. Saito, T. Ajiro, and K. Yoshimura, J. Phys. Soc. Jpn. **75**, 113601 (2006).
- ²² M. Yoshida, N. Ogata, M. Takigawa, J. Yamaura, M. Ichihara, T. Kitano, H. Kageyama, Y. Ajiro, and K. Yoshimura, J. Phys. Soc. Jpn. **76**, 104703 (2007); arXiv:0706.3559.
- ²³ A. A. Tsirlin, A. A. Belik, R. V. Shpanchenko, E. V. Antipov, E. Takayama-Muromachi, and H. Rosner, Phys. Rev. B **77**, 092402 (2008); arXiv:0801.1434.
- ²⁴ K. Oka, I. Yamada, M. Azuma, S. Takeshita, K. H. Satoh, A. Koda, R. Kadono, M. Takano, and Y. Shimakawa, Inorg. Chem. **47**, 7355 (2008).
- ²⁵ E. E. Kaul, H. Rosner, N. Shannon, R. V. Shpanchenko, and C. Geibel, J. Magn. Magn. Mater. **272-276**, 922 (2004).
- ²⁶ E. E. Kaul, PhD thesis, Technical University Dresden, Dresden (2005). Electronic version available at: <http://hsss.slub-dresden.de/documents/1131439690937-4924/1131439690937-4924.pdf>
- ²⁷ M. Skoulatos, J. P. Goff, N. Shannon, E. E. Kaul, C. Geibel, A. P. Murani, M. Enderle, and A. R. Wildes, J. Magn. Magn. Mater. **310**, 1257 (2007).
- ²⁸ M. Skoulatos. Abstracts of the 4th European conference on Neutron scattering in Lund, Sweden, p. 164 (2007).
- ²⁹ A. A. Tsirlin, R. Nath, C. Geibel, and H. Rosner, Phys. Rev. B **77**, 104436 (2008); arXiv:0802.2293.
- ³⁰ A. A. Tsirlin and H. Rosner, unpublished results on the band structures of the AA'VO(PO₄)₂ compounds.
- ³¹ S. Meyer, B. Mertens, and Hk. Müller-Buschbaum, Z. Naturforsch. **52b**, 985 (1997).
- ³² Our results are somewhat different from that of Meyer *et al.*³¹ who report the preparation of single crystals at 975 °C (i.e., above the decomposition temperature of 900 °C observed in our experiments). The origin of this discrepancy is not yet clear. We should emphasize that Meyer *et al.*³¹ report the preparation of small single crystals only. No information about the synthesis and thermal properties of bulk samples of BaCdVO(PO₄)₂ is available.
- ³³ G. J. Hyland, J. Phys. C **1**, 189 (1968).
- ³⁴ The standard deviations for the exchange integrals originate from the fitting procedure only. Varying the lower limit of the data used, one finds a more pronounced change of J 's, and the actual error bar is of the order of 0.1 K.
- ³⁵ We define the saturation field H_s as a point of the maximum negative curvature of the $M(H)$ curve.
- ³⁶ Note that we observe a similar ($\sim 7\%$) reduction of the magnetic entropy in our specific heat data.
- ³⁷ N. S. Kini, E. E. Kaul, and C. Geibel, J. Phys.: Condens. Matter, **18**, 1303 (2006).
- ³⁸ R. Nath, A. A. Tsirlin, E. E. Kaul, M. Baenitz, N. Büttgen, C. Geibel, and H. Rosner, Phys. Rev. B **78**, 024418 (2008), arXiv:0804.4667.
- ³⁹ M. S. Makivić and H.-Q. Ding, Phys. Rev. B **43**, 3562 (1991).
- ⁴⁰ J.-K. Kim and M. Troyer, Phys. Rev. Lett. **80**, 2705 (1998).
- ⁴¹ M. Hofmann, T. Lorenz, K. Berggold, M. Grüninger, A. Freimuth, G. S. Uhrig, and E. Brück, Phys. Rev. B **67**, 184502 (2003).